ELSEVIER

Surface Science 504 (2002) 271–281

SURFACE SCIENCE

www.elsevier.com/locate/susc

STM study of Cu growth on the ZnO(1 0 $\bar{1}$ 0) surface

Olga Dulub [a], Lynn A. Boatner [b], Ulrike Diebold [a,*]

[a] *Department of Physics, Tulane University, New Orleans, LA 70118, USA*
[b] *Oak Ridge National Laboratory, Oak Ridge, TN 37831, USA*

Received 21 August 2001; accepted for publication 21 December 2001

Abstract

The room temperature growth of Cu islands on the non-polar (1 0 $\bar{1}$ 0) surface of zinc oxide was studied using scanning tunneling microscopy. Images of the clean (1 0 $\bar{1}$ 0) surface prepared by sputtering and annealing at 550–700 °C exhibit flat terraces with a high density of steps, mostly running along [0 0 0 1] and [1 $\bar{2}$ 1 0] directions. For Cu coverages of 0.025–1 ML deposited on flat, freshly annealed surfaces, preferential nucleation occurs at the step edges oriented perpendicular to the [1 $\bar{2}$ 1 0] atomic row direction. Exclusively three-dimensional (3D) islands have been observed at all coverages. For comparison, the same Cu coverages were deposited onto the surface contaminated by adsorption from the residual gas in the ultrahigh vacuum chamber. Both 2D and 3D islands, randomly distributed across the terraces, were observed reproducibly on such slightly contaminated surfaces. The density of the islands, as well as their average diameter and height, increases with increasing Cu coverage for both surface preparations. © 2002 Elsevier Science B.V. All rights reserved.

Keywords: Scanning tunneling microscopy; Growth; Adsorption kinetics; Nucleation; Zinc oxide; Copper; Surface defects; Diffusion and migration

1. Introduction

The growth of Cu on ZnO surfaces is a subject of continuing interest due to the importance of Cu as a promoter in the low-temperature synthesis of methanol, water–gas shift reaction, and methanol steam reforming [1]. In addition, this system has become a model for the initial two-dimensional (2D) growth observed for metal overlayers on many metal oxide surfaces. This growth mode occurs for systems that thermodynamically prefer 3D island growth even at the smallest coverages (Vollmer–Weber growth mode). However, 2D growth is observed up to a certain critical island size due to kinetic limitations at low temperatures [2]. This shows the importance of the kinetics of metal adatom diffusion along oxide surfaces, since it can control the growth mode of the adsorbate and prevent the thermodynamically most stable structures from being formed.

Copper growth on different faces of ZnO has been studied extensively in the past using surface analysis techniques such as X-ray photoelectron spectroscopy (XPS) [3], low energy ion scattering

* Corresponding author. Tel.: +1-504-862-8279; fax: +1-504-862-8702.
E-mail address: diebold@tulane.edu (U. Diebold).

0039-6028/02/$ - see front matter © 2002 Elsevier Science B.V. All rights reserved.
PII: S0039-6028(02)01107-X

(LEIS) [3], electron energy loss spectroscopy [4,5], and others. The initial stage of growth (i.e. up to a coverage of several monolayers) is still somewhat controversial. Although there is a general agreement that Cu grows in an island mode, what dimensions the clusters have and how their morphology depends on sample orientation and preparation is still debated. In an early study of Cu growth on different ZnO surfaces, it was reported that the first monolayer wets the oxide substrate [4]. More recent studies of the same systems indicated that the admetal grows two-dimensionally only to a certain critical coverage, at which point it starts to form 3D islands [3,6,7]. Although the general features of the growth mode on Zn- and O-terminated surfaces are similar, there are differences as well. The critical coverage, where islands start to grow three-dimensionally, is approximately twice as high for the O face than for the Zn face under the same conditions [3,7]. This difference could be ascribed to the different defect densities and, therefore, different nucleation center densities of the faces. It could also be related to the different strengths of Cu bonding to the two faces and, therefore, different Ehrlich–Schwoebel barriers (and different sizes of 2D Cu islands at the critical coverage) [8,9]. In any case, different surface structures of the ZnO crystal faces clearly result in different critical coverage values.

In terms of structural resolution and real-space probing, scanning tunneling microscopy (STM) is the most powerful technique, and a direct imaging study could contribute to resolving the discrepancy in the results of different studies. However, as far as we know, metal growth on ZnO has not been studied with STM before. STM data are scarce even for clean polar and non-polar ZnO surfaces [10,11]. It is extremely difficult to achieve atomic-scale resolution, mostly due to the poor conductivity of ZnO samples. In principle, atomic force microscopy (AFM) could be a useful tool here, since it does not rely upon the conductivity of the sample. However, previous studies have shown that metal islands on insulators are often too mobile for the contact AFM mode [12]. The interactions between the metal islands and the AFM tip are significant even in the non-contact AFM mode [13].

In this work, STM has been used to study the initial stage of Cu deposition on the ZnO$(1\,0\,\bar{1}\,0)$ surface, as well as post-annealing effects. We found clear evidence for the influence of substrate preparation on Cu growth and on the critical coverage for the 2D–3D transition.

2. Experimental

The experiments were carried out in an ultra-high vacuum (UHV) chamber with a base pressure of less than 1×10^{-10} mbar. The chamber is equipped with the experimental facilities for low-energy He^+ ion scattering spectroscopy (LEIS), low-energy electron diffraction (LEED), and STM.

The ZnO sample was taken from a single crystal grown in the form of a hexagonal prism. The $(1\,0\,\bar{1}\,0)$-oriented prism face was studied without any ex situ treatment. It was cleaned by cycles of Ar^+ ion bombardment (1 keV) at room temperature (RT) and annealing up to 700 °C. Surface cleanliness and surface ordering were probed with LEIS and LEED, respectively. A well-defined (1×1) LEED pattern was observed on the clean surface. The sample was heated radiatively, and its temperature was monitored by a thermocouple spot-welded on the sample holder.

Cu was vapor deposited onto the clean sample at RT using a home-made evaporation source. A piece of Cu wire (99.999% purity) was placed in a 3×3 mm Ta basket spot-welded to a tungsten wire. Both ends of the wire were connected to electrodes, and the basket temperature was monitored with a thermocouple. A current of 6.5 A was used to heat the basket from RT to the evaporation temperature of 1100 °C. The sample was placed approximately 10 cm away from the evaporator during the Cu evaporation. The pressure during Cu deposition remained below 2×10^{-10} mbar, which is only slightly higher than the normal operating pressure. A deposition rate of 0.0013 Å s^{-1} was used in all the experiments. The deposition rate was calibrated by a quartz crystal microbalance before growth and checked with STM by statistical analysis of the island densities

and heights. The height of the clusters at the step edges was measured from the top of each cluster to the lower terrace. The width was measured on the cluster's profile cross-section between the points on the base line where the profile line starts to bend upwards. The tip convolution effect due to the finite size of the STM tip was taken into account by simply using the tables of Ref. [14]. The concentration of the deposited metal is given in the monolayer equivalent (ML), which corresponds to the Cu(1 1 1) packing density of 1.7×10^{15} Cu atoms per cm^2. The expected thickness of one layer of Cu(1 1 1) is 2.2 Å. All STM data were recorded in the constant-current mode at a positive sample bias of 1.5–2.5 V and with a feedback current of 0.8–1.8 nA.

During the course of the experiments, it was found that the exposure of the clean surface to the residual gas in the UHV chamber has a pronounced effect on Cu growth. In order to study this effect systematically, two sets of data are presented. For the first set, the sample surface was kept as clean as possible before the Cu evaporation. Our setup does not allow for a rapid cooling of a hot sample, so there is a minimum waiting period of 45 min to ensure that Cu deposition was performed at RT. It takes an additional 2 min to transfer the sample to the STM and 30 min to take a data set. The results shown here were for cumulative Cu depositions, without cleaning the sample in between. They do not differ substantially from the control experiments, where a similar Cu loading was deposited in one step. All the filaments in the chamber were turned off while cooling the sample. The residual gas pressure in the chamber was 2×10^{-10} mbar under that condition. The second set of data was taken on the sample prepared by sputtering and annealing in the same way. The clean surface was exposed to a very similar Cu flux rate and dosage. However, the sample was kept in a background pressure of 5×10^{-10} mbar for 3 h before the evaporation, with the ion pump turned off and filaments turned on. This procedure mimics Cu deposition under "not-ideal" (but not untypical) vacuum conditions. This prolonged exposure to the residual gas in the chamber substantially affects the Cu growth.

3. Results

3.1. Clean ZnO(1 0 $\bar{1}$ 0) surface

Fig. 1 shows STM images of the clean ZnO-(1 0 $\bar{1}$ 0) surface prepared by sputtering and annealing in UHV at 700 °C for 20 min. A number of flat terraces separated by monatomic steps running along either [0 0 0 1] (type A) or [1 $\bar{2}$ 1 0] (type B) directions can be seen (Fig. 1a). The geometry of these two step types is discussed below. The average step height is 3 Å, which agrees well with the expected vertical separation of two consecutive ZnO planes (2.8 Å). On the smaller scale image (Fig. 1b), near-atomic resolution shows bright and dark rows running along the [1 $\bar{2}$ 1 0] direction. These rows are associated with ZnO-dimers aligned in this direction. The resolution in this image is not high enough to distinguish single atoms. Based

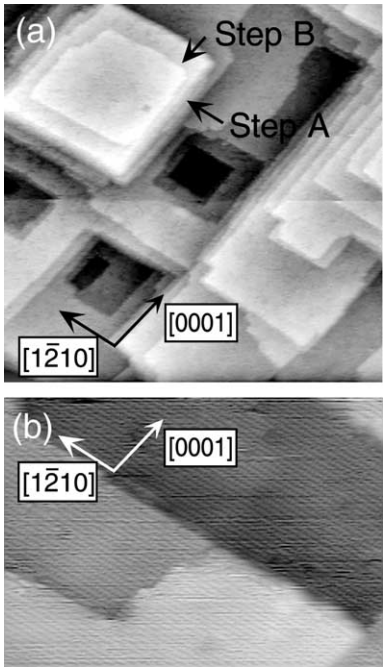

Fig. 1. STM images of the clean ZnO(1 0 $\bar{1}$ 0) surface: (a) wide-scale image (1000×1000 Å^2, +1.8 V, 1.46 nA) showing flat terraces separated by two types of step edges; (b) near atomic-resolution image (250×250 Å^2, +2.1 V, 0.8 nA) showing bright and dark rows running along the [1 $\bar{2}$ 1 0] direction. The surface has been prepared by sputtering and annealing in UHV at 700 °C for 20 min.

on the surface morphology, one would expect to image the O atoms (they are located 0.4 ± 0.2 Å above Zn in the $(1\,0\,\bar{1}\,0)$ plane [15]), while the positive sample bias in the STM measurements makes it more probable that the bright rows consist of Zn ions. These results in Fig. 1 are in good agreement with a previous STM study of a clean ZnO$(1\,0\,\bar{1}\,0)$ surface, see Ref. [11].

3.2. Cu growth on a clean ZnO$(1\,0\,\bar{1}\,0)$ surface

In this series of experiments, the clean sample was prepared as described above. The STM images of the surface after deposition of 0.025 ML of Cu are shown in Fig. 2a. The step edges are decorated with bright spots that are associated with Cu clusters. Nucleation occurs mostly along the edges of type A steps. A number of step edges that are not perpendicular to either major direction of the surface is observed. These are also populated with Cu clusters. Very few clusters are seen along the type B steps running parallel to the dimer rows. Also, very few clusters are located on the terraces away from the step edges, and those that are present are located primarily on the top-most terraces. The inset in Fig. 2a shows a series of three narrow terraces labeled 1–3. Interestingly, nucleation occurs at the lowest step edge ($3 \rightarrow 2$), but no clusters are observed at the center terrace (2). All clusters are well separated and appear to have the same round shape. However, their exact shape is hard to determine due to the tip-convolution effect. From the STM images like those in Fig. 2a, we have selected a set of well-separated Cu islands (176 at the step edges and 37 on the terraces). The diameter of each cluster was measured from two perpendicular cross-sections, and the values obtained were averaged. The average measured height of the clusters is 6–9 Å, which corresponds to the thickness of 2–3 layers of Cu. The diameter ranges from 15 to 40 Å (Fig. 2c). (These and the subsequent numbers were not corrected for the tip convolution effect.) The line profile of one of these clusters is shown in Fig. 2b. Clearly, even at a coverage as low as 0.025 ML, clusters grow exclusively three-dimensionally.

Fig. 3 shows that as more Cu is deposited on the surface (0.05–0.5 ML), the concentration of clusters increases rapidly while their average size grows more slowly. The density of clusters at 0.5 ML coverage is about three times as large as that at 0.05 ML. For each coverage, the average cluster size is the same at the step edges and on the terraces. The average cluster heights are 7.2, 8.9, 11.8, and 14 Å, and the average cluster diameters are 34, 36, 38, and 45 Å at 0.05, 0.1, 0.25, and 0.5 ML coverage, respectively. As the type A step edges saturate with clusters, new clusters start to nucleate on terraces and then on type B step edges. Thus, Cu nucleates on the surface in the following order: along the $(1\,\bar{2}\,1\,0)$ steps $\rightarrow$ on the terraces $\rightarrow$ along the $(0\,0\,0\,1)$ steps.

3.3. Cu growth on the slightly contaminated ZnO-$(1\,0\,\bar{1}\,0)$ surface

In the experiments described in this section, the sample preparation described above was used.

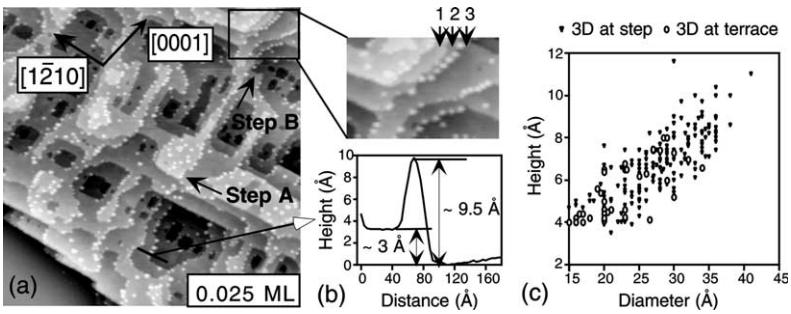

Fig. 2. (a) STM image (2000×2000 Å^2) after the deposition of 0.025 ML of Cu at RT on a clean ZnO$(1\,0\,\bar{1}\,0)$ surface, prepared as in Fig. 1; (b) island height vs. diameter plot for a set of 176 Cu islands at the steps and 37 Cu islands on terraces; (c) line-profile plot showing the width and the height of a Cu island as indicated in (a).

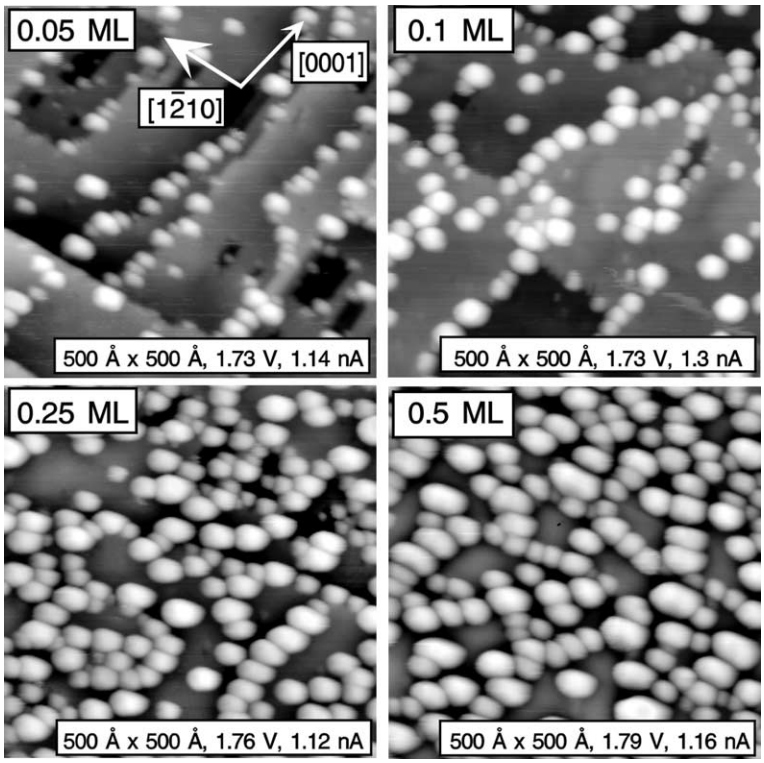

Fig. 3. STM images for various Cu coverages (0.05–0.5 ML) on the ZnO(1 0 $\bar{1}$ 0) surface, prepared under the same conditions as in Fig. 2.

However, before Cu was deposited, the sample was exposed to the residual gas in the chamber, as described in Section 2. Cu was then deposited under the same conditions as before, and STM images were taken. The mode of cluster growth and distribution of nucleation centers is very different from the previous experiment. As shown in Fig. 4, in the whole range of coverages (0.03–0.06 ML), Cu clusters are randomly distributed across the substrate and no preferential nucleation sites are observed. The line profile of two neighboring islands from the STM image taken at 0.025 ML coverage reveals the presence of the 2D islands, which were completely absent in the low-nucleation site density-case described in Section 3.2.

The change in the number of 2D and 3D islands on the surface with coverage increase is shown in Fig. 5. At the smallest coverage (0.03 ML), clusters grow mostly two-dimensionally on the terraces, and only a few 3D clusters are observed on the terraces and at the step edges. As the coverage increases, the number of 2D islands decreases and more 3D clusters appear. At the coverage of 0.06 ML mostly 3D clusters are present. Fig. 5 also shows that, in contrast, for Cu growth on a clean ZnO surface, no 2D clusters are present at the same coverage. It should be emphasized that the observed effects were reproduced several times. The big differences in the growth morphology displayed in Figs. 2 and 3 are clearly attributable to the exposure to the residual gas and not to small variations in the surface preparation parameters such as sputtering or annealing temperature and time.

3.4. The effects of post-annealing of the Cu/ZnO growth

Finally, we investigated the effect of post-annealing of the Cu films on a ZnO(1 0 $\bar{1}$ 0) surface.

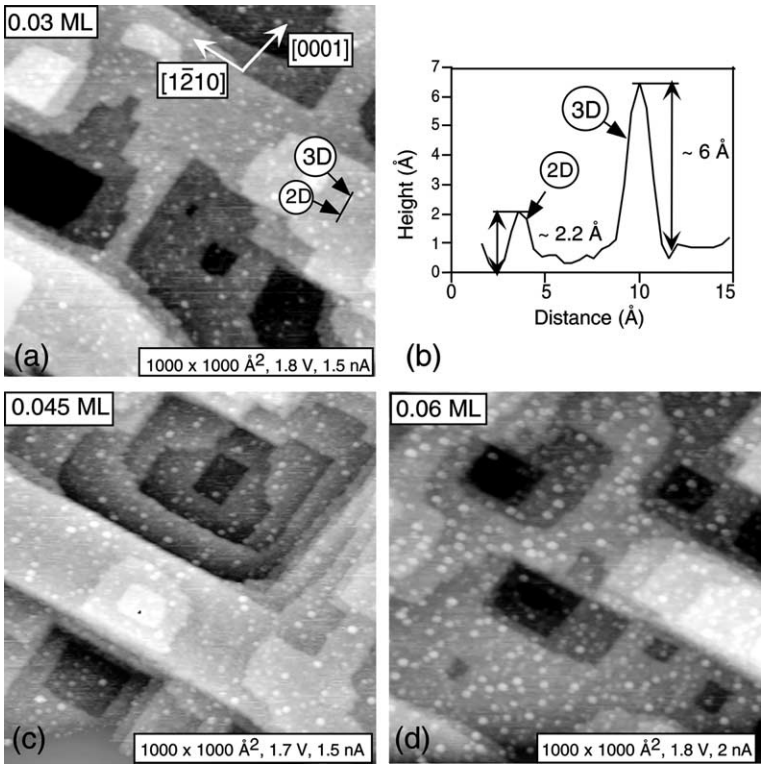

Fig. 4. (a, c, d) STM images showing the growth of Cu on a slightly contaminated ZnO(1 0 $\bar{1}$ 0) surface (same preparation as in Fig. 2, but exposed to the residual gas at 5×10^{-10} mbar for 3 h); (b) the profile plot along the line in (a) shows 2D and 3D islands.

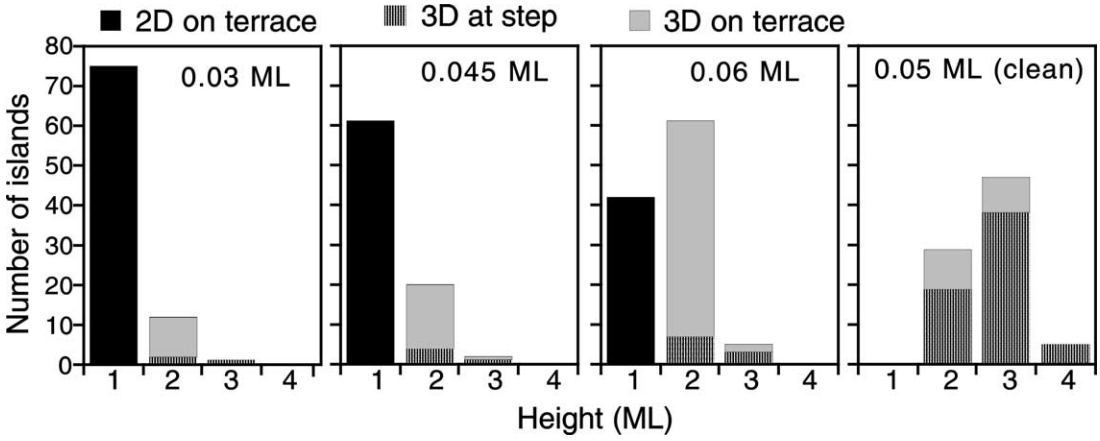

Fig. 5. Histograms of island-height distributions for various Cu coverages deposited on the slightly contaminated ZnO(1 0 $\bar{1}$ 0) surface and on the clean surface (last histogram). Areas of 560×560 Å^2 were evaluated.

Fig. 6 shows the result of annealing the Cu/ZnO system, prepared as in Fig. 4a, for 5 min at 450 °C. The density of clusters decreases drastically as large 3D islands are formed. The average island

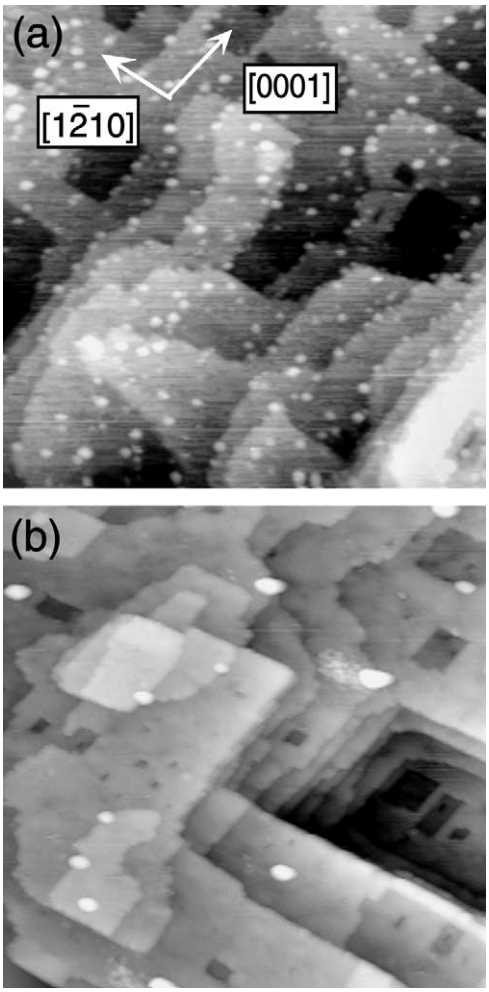

Fig. 6. STM images (1000 × 1000 Å^2) (a) after deposition of 0.025 ML of Cu at RT on a slightly contaminated surface, (b) followed by annealing at 450 °C for 5 min.

dimensions are 15–20 Å (≈7–10 layers of Cu) in height and 40–45 Å in diameter.

4. Discussion

As can be seen from Fig. 2, Cu clusters grow three-dimensionally even at very small coverages (0.025 ML) on a (nearly perfect) surface. Annealing the surface at a high temperature (5 min at 450 °C) results in the aggregation of all small clusters to form a few large ones (Fig. 6). Both these observations suggest a weak interaction between the Cu adatoms and the oxide substrate and a high mobility of Cu at elevated temperatures.

Inspection of the distribution of the Cu cluster nucleation sites under different preparation conditions results in two interesting observations. First, on clean surfaces prepared under conditions of low exposure to the residual gas of the chamber, nucleation of exclusively 3D islands is strongly preferred along the step edges running perpendicular to the [1 $\bar{2}$ 1 0] direction as well as the step edges cutting across the rows of dimers. At low coverages, no nucleation is observed along the step edges running parallel to the [1 $\bar{2}$ 1 0] direction (Fig. 2). Second, the presence of adsorbates on the surface drastically changes the Cu growth mode, as it removes any preference in nucleation site distribution and allows 2D growth (Fig. 4). Before discussing these results, it is useful to recall the geometric structure of ZnO(1 0 $\bar{1}$ 0).

In general, the clean ZnO(1 0 $\bar{1}$ 0) surface observed in our experiments corresponds well with the previous experimental and theoretical data [11,16]. The geometry of a terrace on top of a ZnO(1 0 $\bar{1}$ 0) surface is shown in Fig. 7. The concept of autocompensation [17] is useful for predicting the step geometry on metal oxides with a high degree of covalent character [18]. The (1 0 $\bar{1}$ 0) surface itself is autocompensated since it has an equal number of Zn and O ions per unit area and only one bond per atom is broken when the surface is created. The type A and B step faces consist of stable low Miller index ($\bar{1}$ 2 $\bar{1}$ 0) and (0 0 0 1) planes, correspondingly. The ($\bar{1}$ 2 $\bar{1}$ 0) face of type A steps is also an autocompensated surface, whereas the (0 0 0 1) faces of type B steps are polar and have either zinc or oxygen termination. One could expect that the different step edges exhibit different chemical reactivities, which could affect the nucleation mechanisms. However, this is clearly not the case in our study, since both kinds of type B step edges are not decorated with clusters, although they have a very different termination. Thus, kinetics are essential for the Cu/ZnO system.

As shown in Fig. 7a, the oxygen atoms in the top-most layer are slightly elevated above the Zn atoms in the dimers. This creates "trenches"

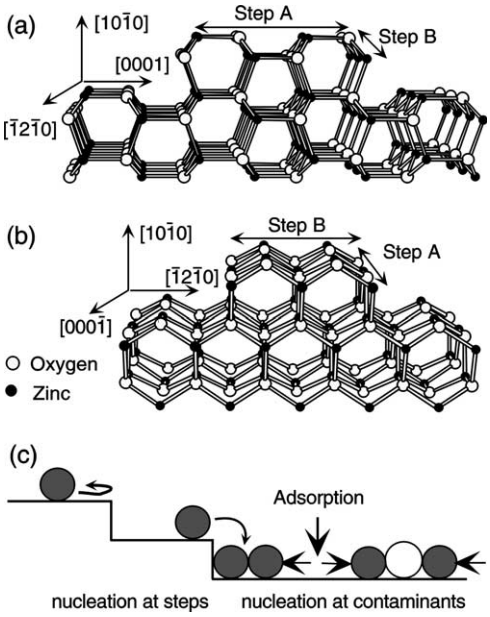

Fig. 7. (a, b) Perspective views of the bulk-terminated ZnO crystal. Two major step orientations are shown: perpendicular to the dimer rows (step A, in the plane of the picture) and parallel to the dimer rows (step B, into the plane of the picture). Notice the two different terminations of the B steps. "Trenches" of dimer rows run along the [$\bar{1}$ 2 $\bar{1}$ 0] direction. Secondary Cu diffusion trenches run along A step edges in the [0 0 0 1] direction. (c) Schematics of the proposed nucleation mechanisms.

(channels between dimer rows) running along the [$\bar{1}$ 2 $\bar{1}$ 0] direction. Only type A steps, as well as steps cutting across the dimer rows, are populated with clusters. This suggests that diffusion of Cu along the surface is much faster along the [$\bar{1}$ 2 $\bar{1}$ 0] direction than along [0 0 0 1], as if Cu adatoms were confined to move along the trenches. When an adatom on an upper terrace encounters a down-step, it could jump to the lower terrace across the step. Alternatively, if its diffusion energy is less than the Ehrlich–Schwoebel barrier [8,9], it would be reflected from the step edge. Then only adatoms bumping into an up-step when moving along the [$\bar{1}$ 2 $\bar{1}$ 0] direction on the lower terrace would contribute to cluster nucleation. The second scenario is more likely during initial stages of the step decoration process. This is confirmed by the observation that the number of islands at the step edges is roughly proportional to the area of the terrace on the lower and not the upper side of the step edge. Consider, for example, terraces 1, 2, and 3 on the inset of Fig. 2a. The step edge between terraces 1 and 2 is not decorated with islands, since terrace 2 is too narrow to have enough adatoms of its own. The step edge between terraces 2 and 3, on the other hand, is populated since terrace 3 is wide and collects sufficient adsorbed Cu. When an adatom approaches the step edge from the lower terrace side, it is easily incorporated into the step edge since this is an energetically favorable high-coordinated adsorption site. Such adatoms now act as nucleation sites and they trap incoming Cu atoms from both the lower and upper terraces. Due to strong Cu–Cu interaction, the Ehrlich–Schwoebel barrier at the nucleation sites becomes lower. Therefore, adatoms incoming from the upper terrace can now jump down and contribute to the 3D growth of clusters even at the smallest coverages (Fig. 7c). Moreover, adatoms incoming at the step edge along the trench can "see" clusters nucleated at the neighboring trenches, also due to the strong Cu–Cu interaction. They can migrate in the [0 0 0 1] direction along step A, as shown in Fig. 7b—also contributing to the 3D growth of the islands.

A few islands were observed on terraces. This could be due to defects that act as nucleation sites or to a nucleation mechanism where two diffusing Cu adatoms meet. The former is hardly the case, although the influence of point defects on nucleation-site distributions was demonstrated in the case of Pd deposited onto a TiO_2(1 1 0) surface [19]. It was shown that on a mildly reduced titania surface Pd, nucleates preferentially at the step edges, whereas on a strongly reduced sample Pd nucleated on the terraces as well. However, we exclude the effect of point defects in the Cu/ZnO experiment, since previous studies indicate that annealing of a stoichiometric ZnO(1 0 $\bar{1}$ 0) surface even at temperatures higher than 700 K produces negligibly small O-vacancy defect concentrations ($\leqslant 1 \times 10^{-4}$ ML) [20], and we observed both preferential and random nucleation site distribution on samples prepared with the same heat treatment procedure. The second nucleation mechanism is supported by observations of increased Cu island concentration on the top-most terraces (Fig. 2a).

The probability of two Cu adatoms meeting each other is increased on the top-most terraces, since they reflect off of the Ehrlich–Schwoebel barrier at the step edge. They do so until they bind either to another diffusing adatom on the top-most terrace or with the Cu atoms incorporated at the step edge from below. These islands also grow three-dimensionally from the very beginning (0.025 ML).

The influence of the residual gas pressure on metal overlayer growth on metallic surfaces has been studied only recently [21]. Unfortunately, such contaminants are very hard to detect on the surface with the techniques available to us. The main components of the residual gas and corresponding exposures (3 h at 5×10^{-10} mbar) were H_2O (44% and 2 Langmuir (L)), CO (40% and 2 L), H_2 and CO_2 (7% and 0.3 L each). Thus, the total exposure was 5 L, which is 24 times larger than the 0.2 L exposure under normal operating conditions (45 min at 10^{-10} mbar). Any of these contaminants could affect Cu nucleation and growth on ZnO in different ways. Adsorbed gas molecules

(i) at step edges can prevent Cu adatoms from nucleating at these preferred sites;
(ii) can act as additional sites for Cu cluster nucleation; or
(iii) can affect Cu–Cu and Cu–substrate interactions and, thus, the mobility of Cu on the surface.

The interaction of each of the main constituents of the residual gas (CO, CO_2, H_2O, and H_2) with the ZnO(1 0 $\bar{1}$ 0) surface and with Cu was evaluated from literature data in order to assess their influence on the nucleation process.

A number of research groups have studied CO and CO_2 adsorption on clean ZnO surfaces at different temperatures with a variety of techniques. Angle-resolved photoelectron spectroscopy [22, 23], ultraviolet photoelectron spectroscopy (UPS) [24], and He-II valence band measurements [4] clearly indicated that CO binds to the Zn site carbon-end-down on the ZnO(1 0 $\bar{1}$ 0) surface at low temperatures (<200 K). [22]. This was also confirmed by theoretical cluster calculations [25, 26]. Carbon monoxide displacement from the surface by the residual H_2O was observed at 77 K [22]. CO adsorption at RT is very weak on the ZnO(1 0 $\bar{1}$ 0) surface. The increase in electrical conductivity and electronic work function and the results of subsequent thermal desorption measurements upon CO exposure on ZnO(1 0 $\bar{1}$ 0) at RT were interpreted in terms of the formation of chemisorbed CO_2 and O vacancies at the surface [27]. Thermal desorption experiments after RT CO adsorption on the stoichiometric (1 0 $\bar{1}$ 0) surface found CO_2 desorption peaks [27–29]. The CO exposure and corresponding coverage in these experiments were ~1 L (1.33×10^{-5} Pa for 2 min) and 2.5×10^{-4} ML. The estimated exposure for the case of a 'slightly contaminated' surface was twice as much, thus it is feasible that CO adsorption plays a role in the Cu nucleation. However, CO adsorption on ZnO(1 0 $\bar{1}$ 0) at RT was reported as undetectable in Ref. [30].

CO_2 can exist on ZnO(1 0 $\bar{1}$ 0) in both weakly ("physisorbed") and strongly ("chemisorbed") bound states [31]. The reversible adsorption and desorption of CO_2 at 298–473 K with a sticking coefficient of 0.6 was found on the stoichiometric (1 0 $\bar{1}$ 0) surface [27]. Thermal desorption measurements were performed on ZnO after CO_2 exposure at $P = 1.33 \times 10^{-5}$ Pa for 2 min (1 L and 1.4×10^{-2} ML) [29]. Three CO_2 desorption peaks associated with different adsorption sites were observed. Interestingly, the intensity of the CO_2 desorption peak was found to depend strongly on the cooling time before adsorption (10 min to 12 h waiting time with the base pressure of 10^{-8} Pa). This was attributed to the amount of the adsorbed residual H_2O.

H_2O adsorbs on ZnO(1 0 $\bar{1}$ 0) at low temperature (130 K) with a sticking probability close to 1 [32]. The adsorption of H_2O on ZnO(1 0 $\bar{1}$ 0) at low temperature was studied in thermal desorption and UPS experiments [33]. At monolayer coverage, the binding to Zn sites was found to be stronger than to O sites. No detectable H_2O adsorption was observed at RT [32].

Molecular hydrogen does not interact with ZnO surfaces at low partial pressures. Its sticking coefficient is small compared to that of atomic hydrogen, and dissociative adsorption is significant

only at high concentrations (one H_2 molecule per Zn–O dimer on the surface) [34]. Under UHV conditions, no dissociative adsorption of H_2 was found [30]. Atomic hydrogen interacts strongly with ZnO(1 0 $\bar{1}$ 0), acting as a donor. It should be mentioned that the filament of an ion gauge, which can produce atomic hydrogen from H_2 in the UHV environment, was left on during this part of the experiment. The interaction of atomic hydrogen with stoichiometric ZnO(1 0 $\bar{1}$ 0) has been studied theoretically by means of cluster calculations [34,35]. The H adsorption is believed to occur at surface zinc and oxygen atoms. The O–H bond is strong compared with the O–metal bond in the bulk of the oxide.

Oxygen constitutes only a small fraction (<0.3%) of the residual gas in the chamber and was found to adsorb on ZnO with very low sticking probability [16,32]. Therefore, its effects on the processes on the surface are neglected.

The cited literature data on the adsorption of the different gases partially contradict each other, and it is not straightforward to conclude which one, or which combination, of the relevant gases, affects the Cu nucleation the most. However, CO and/or CO_2 are the most likely candidates as both gases interact strongly with Cu supported on ZnO. It is generally agreed that CO chemisorbs on a Cu-promoted catalyst more strongly than on a clean ZnO surface. The nature of active sites on such catalysts is not very well understood. It has been proposed that Cu^+ are the active centers for CO adsorption and methanol synthesis [36–38]. Studies using LEED, work function measurements, ion-scattering spectroscopy, and XPS demonstrated that Cu is cationic at very low coverages [3,5,38]. However, another electron spectroscopy experiment showed that even at very low coverages, Cu can be mostly in the metallic state. A submonolayer of Cu on the ZnO(1 0 $\bar{1}$ 0) surface can drastically enhance its ability to adsorb CO with the binding energy of CO similar to that on metallic Cu surfaces [39]. A theoretical study of CO on clean and Cu-doped ZnO(1 0 $\bar{1}$ 0) also indicated that the ZnO–CO interaction is much weaker than the Cu–CO bonding [40]. Thus, small amounts of CO on the surface would present favorable nucleation sites for Cu (process (ii), see Fig. 7c). If one assumes that each Cu cluster on a terrace has nucleated at one adsorbed CO molecule, the corresponding CO coverage for a typical data set (e.g., the first histogram in Fig. 5) would amount to 5×10^{-3} ML. The sample was exposed to 2 L CO, thus a very small sticking coefficient is needed to yield the inferred number of adsorption sites. An inactivation of step edges by adsorbed CO molecules (process (i)) is probably a minor effect, since CO was shown to nucleate on terraces rather than at step edges [23]. CO_2 was also shown to nucleate on (1 0 $\bar{1}$ 0) terraces rather than at steps with Zn edge atoms (type B steps) [16].

'Surfactant' experiments support the conjectured role of CO on the adsorption and nucleation process. On polar (0 0 0 1) faces of ZnO, vapor-depositing Cu in the presence of CO in the gas phase was found to cause the metal islands to spread more effectively and cover a larger fraction of the substrate [41]. Similar effects were reported for Pt deposition on TiO_2(1 1 0) [42]; Pt on Pt(1 1 1) [21]; Ir on TiO_2(1 1 0)-(1 × 2) [43,44]; and Al on NiAl(1 1 0) with subsequent exposure to water [45]. An energetic model proposed by Ernst et al. argues that this effect is thermodynamically reasonable [3].

5. Conclusion

Cu nucleation on the ZnO(1 0 $\bar{1}$ 0) surface depends strongly on surface defects such as step edges and adsorbates. On clean surfaces, clusters grow almost exclusively three-dimensionally at the step edges oriented perpendicular to the [1 $\bar{2}$ 1 0] direction from the lowest coverages, while the terraces remain mostly free of islands. Selective clustering of Cu along the non-polar [1 $\bar{2}$ 1 0] steps suggests that Cu adatoms diffuse on the surface preferentially along the [1 $\bar{2}$ 1 0] direction until they are stopped at the step edges or other defect sites. Further growth of Cu suggests preferential nucleation in the following order: along the (1 $\bar{2}$ 1 0) steps → on the terraces → along the (0 0 0 1) steps. In contrast, surfaces contaminated with residual gas from the UHV chamber reveal the nucleation and growth of both 2D and 3D clusters randomly distributed across the entire surface. It is proposed

that a strong interaction of Cu with adsorbed CO and/or CO_2 molecules causes a decrease in diffusion length, possibly by providing stable nucleation sites at the flat terraces. This is the first observation of such a dramatic influence of the residual gas at such small pressure on the metal/oxide growth mode, and it shows the importance of surface preparation for metal/oxide experiments. Impurities from the residual gases in a UHV chamber can affect the experimental results dramatically—yet, they are very hard to avoid.

Acknowledgements

This work was supported by NSF (CHE-0109804). ORNL is supported by the US DOE-BES under contract no. DE-AC05-96OR22464. We thank Dr. Wilhelm Hebenstreit for help and useful discussions.

References

[1] C.N. Satterfield, Heterogeneous Catalysis in Industrial Practice, McGraw-Hill, 1991.
[2] C.T. Campbell, A. Ludviksson, J. Vac. Sci. Technol. A 12 (1994) 1825.
[3] K.H. Ernst, A. Ludviksson, R. Zhang, J. Yoshihara, C.T. Campbell, Phys. Rev. B: Condens. Matter 47 (1993) 13782.
[4] S.V. Didziulis, K.D. Butcher, S.L. Cohen, E.I. Solomon, J. Am. Chem. Soc. 111 (1989) 7110.
[5] J.W. He, P.J. Møller, Surf. Sci. 180 (1987) 411.
[6] C.T. Campbell, Surf. Sci. Rep. 27 (1997) 1.
[7] J. Yoshihara, J.M. Campbell, C.T. Campbell, Surf. Sci. 406 (1998) 235.
[8] G. Ehrlich, F.G. Hudda, J. Chem. Phys. 44 (1966) 1039.
[9] R.L. Schwoebel, E.J. Shipsey, J. Appl. Phys. 37 (1966) 3682.
[10] P.M. Thibado, G.S. Rohrer, D.A. Bonnell, Surf. Sci. 318 (1994) 379.
[11] T.M. Parker, N.G. Condon, R. Lindsay, F.M. Leibsle, G. Thornton, Surf. Sci. 415 (1998) L1046.
[12] G. Beitel, K. Markert, J. Wiechers, J. Hrbek, R.J. Behm, Springer Ser. Surf. Sci. 33 (1993) 71.
[13] C.L. Pang, H. Raza, S.A. Haycock, G. Thornton, Surf. Sci. 460 (2000) L510.
[14] D.A. Chen, M.C. Bartelt, R.Q. Hwang, K.F. McCarty, Surf. Sci. 450 (2000) 78.
[15] C.B. Duke, R.J. Meyer, A. Paton, P. Mark, Phys. Rev. B: Condens. Matter 18 (1978) 4225.
[16] W.H. Cheng, H.H. Kung, Surf. Sci. 102 (1981) L21.
[17] J.P. LaFemina, Crit. Rev. Surf. Chem. 3 (1994) 297.
[18] U. Diebold, J. Lehman, T. Mahmoud, M. Kuhn, G. Leonardelli, W. Hebenstreit, M. Schmid, P. Varga, Surf. Sci. 411 (1998) 137.
[19] M.J.J. Jak, C. Konstapel, A. van Kreuningen, J. Chrost, J. Verhoeven, J.W.M. Frenken, Surf. Sci. 474 (2001) 28.
[20] W. Göpel, Surf. Sci. 62 (1977) 165.
[21] M. Kalff, G. Comsa, T. Michely, Phys. Rev. Lett. 81 (1998) 1255.
[22] M.J. Sayers, M.R. McClellen, R.R. Gay, E.I. Solomon, F.R. McFeely, Chem. Phys. Lett. 75 (1980) 575.
[23] K.L. D'Amico, M. Trenary, N.D. Shinn, E.I. Solomon, F.R. McFeely, J. Am. Chem. Soc. 104 (1982) 5102.
[24] R.R. Gay, M.H. Nodine, V.E. Henrich, H.J. Zeiger, E.I. Solomon, J. Am. Chem. Soc. 102 (1980) 6752.
[25] J.E. Jaffe, A.C. Hess, J. Chem. Phys. 104 (1996) 3348.
[26] N. Vulliermet, T.A. Wesolowski, J. Weber, Collect. Czech. Chem. Commun. 63 (1998) 1447.
[27] W. Hotan, W. Göpel, R. Haul, Surf. Sci. 83 (1979) 162.
[28] W. Hotan, W. Göpel, R. Haul, Ned. Tijdschr. Vacuumtech. 16 (1978) 61.
[29] W.H. Cheng, H.H. Kung, Surf. Sci. 122 (1982) 21.
[30] Q. Guo, P.J. Møller, Appl. Surf. Sci. 115 (1997) 39.
[31] W. Göpel, R.S. Bauer, G. Hansson, Surf. Sci. 99 (1980) 138.
[32] R. Zhang, A. Ludviksson, C.T. Campbell, Surf. Sci. 289 (1993) 1.
[33] G. Zwicker, K. Jacobi, Surf. Sci. 131 (1983) 179.
[34] P. Zapol, J.B. Jaffe, A.C. Hess, Surf. Sci. 422 (1999) 1.
[35] A. Wander, N.M. Harrison, J. Phys. Chem. B 105 (2001) 6191.
[36] K.R. Harikumar, C.N.R. Rao, Appl. Surf. Sci. 125 (1998) 245.
[37] E.I. Solomon, P.M. Jones, J.A. May, Chem. Rev. 93 (1993) 2623.
[38] K.C. Waugh, Catal. Today 15 (1992) 51.
[39] Q. Ge, P.J. Møller, Appl. Surf. Sci. 82 (1994) 305.
[40] M. Casarin, C. Maccato, A. Vittadini, Appl. Surf. Sci. 142 (1999) 192.
[41] J. Yoshihara, C.T. Campbell, Surf. Sci. 407 (1998) 256.
[42] H.-P. Steinrück, F. Pesty, L. Zhang, T.E. Madey, Phys. Rev. B: Condens. Matter 51 (1995) 2427.
[43] A. Berkó, F. Solymosi, Surf. Sci. 411 (1998) L900.
[44] A. Berkó, F. Solymosi, J. Phys. Chem. B 104 (2000) 10215.
[45] M. Heemeier, M. Frank, J. Libuda, K. Wolter, H. Kuhlenbeck, M. Bäumer, H.J. Freund, Catal. Lett. 68 (2000) 19.